January 2008

CERN-PH-TH/2007-177
SLAC-PUB-12859
ZU-TH 30/07
FERMILAB-PUB-07-639-T
PITHA 07/21
arXiv:0712.3009v1[hep-ph]

Logarithmically Enhanced Corrections to the Decay Rate and Forward Backward Asymmetry in $\bar{B} \to X_s \ell^+ \ell^-$

Tobias Huber[1,2], **Tobias Hurth**[3,4,*], **and Enrico Lunghi**[5]

[1] *Institute for Theoretical Physics, Univ. of Zurich, CH-8057, Zurich, Switzerland.*

[2] *Institut für Theoretische Physik E, RWTH Aachen, D-52056 Aachen, Germany*

[3] *CERN, Dept. of Physics, Theory Division, CH-1211 Geneva, Switzerland.*

[4] *SLAC, Stanford University, Stanford, CA 94309, USA*

[5] *Fermi National Accelerator Laboratory, P.O.Box 500, Batavia, IL 60510, U.S.A.*

Abstract

We study logarithmically enhanced electromagnetic corrections to the decay rate in the high dilepton invariant mass region as well as corrections to the forward backward asymmetry (FBA) of the inclusive rare decay $\bar{B} \to X_s \ell^+ \ell^-$. As expected, the relative effect of these corrections in the high dilepton mass region is around -8% for the muonic final state and therefore much larger than in the low dilepton mass region.
We also present a complete phenomenological analysis, to improved NNLO accuracy, of the dilepton mass spectrum and the FBA integrated in the low dilepton mass region, including a new approach to the zero of the FBA. The latter represents one of the most precise predictions in flavour physics with a theoretical uncertainty of order 5%. We find $(q_0^2)_{\mu\mu} = (3.50 \pm 0.12)\text{GeV}^2$. For the high dilepton invariant mass region, we have $\mathcal{B}(\bar{B} \to X_s \mu\mu)_{\text{high}} = (2.40^{+0.69}_{-0.62}) \times 10^{-7}$. The dominant uncertainty is due to the $1/m_b$ corrections and can be significantly reduced in the future. For the low dilepton invariant mass region, we confirm previous results up to small corrections.

*Heisenberg Fellow

Submitted to Nuclear Instrumentation and Methods (NIM) A

Work supported in part by US Department of Energy contract DE-AC02-76SF00515

1 Introduction

At the beginning of the LHC era, the search for physics beyond the Standard Model (SM) is the main focus of particle physics. In principle, there are two ways to search for possible new degrees of freedom. At the high-energy frontier one tries to produce those new degrees of freedom directly, while at the high-precision frontier one analyses the indirect virtual effects of such new particles. It is a matter of fact that high-precision measurements allow to analyse new physics scales presently not accessible at direct collider experiments.

There are theoretical arguments like the hierarchy problem which let us expect new physics at the electroweak scale. However, the indirect constraints on new physics by the present flavour data indicate a much higher new physics scale when such new effects are naturally parametrized by higher-dimensional operators. Thus, if there is new physics at the electroweak scale, then its flavour structure has to be highly non-trivial and the experimental measurement of flavour-violating couplings is mandatory. This 'flavour problem' has to be solved by any new physics scenario at the electroweak scale. Moreover, the present electroweak data also indicate a slightly higher new physics scale ('little hierarchy problem').

Among inclusive flavour-changing neutral current (FCNC) processes (for a review see [1,2]), the inclusive $\bar{B} \to X_s \ell^+ \ell^-$ decay presents an important test of the SM, complementary to the inclusive $\bar{B} \to X_s \gamma$ decay. It is particularly attractive because of kinematic observables such as the dilepton invariant mass spectrum and the forward-backward asymmetry (FBA). These observables are dominated by perturbative contributions if the $c\bar{c}$ resonances that show up as large peaks in the dilepton invariant mass spectrum are removed by appropriate kinematic cuts. In the so-called 'perturbative q^2-windows', namely in the low-dilepton-mass region $1\,\mathrm{GeV}^2 < q^2 = m_{\ell\ell}^2 < 6\,\mathrm{GeV}^2$, and also in the high-dilepton-mass region with $q^2 > 14.4\,\mathrm{GeV}^2$, theoretical predictions for the invariant mass spectrum are dominated by the perturbative contributions, and a theoretical precision of order 10% is in principle possible.

The integrated branching ratio has been measured by both Belle [3] and BaBar [4] based on a sample of 152×10^6 and 89×10^6 $B\bar{B}$ events respectively. In the low-dilepton invariant mass region, $1\ \mathrm{GeV}^2 < q^2 < 6\ \mathrm{GeV}^2$, the experimental results read

$$\mathcal{B}(\bar{B} \to X_s \ell^+ \ell^-)_{\text{low}} = \begin{cases} \left(1.493 \pm 0.504^{+0.411}_{-0.321}\right) \times 10^{-6} & \text{(Belle)} \\ (1.8 \pm 0.7 \pm 0.5) \times 10^{-6} & \text{(BaBar)} \\ (1.60 \pm 0.50) \times 10^{-6} & \text{(Average)} \end{cases} \tag{1}$$

Measurements for the high-q^2 region, $14.4\ \mathrm{GeV}^2 < q^2 < 25\ \mathrm{GeV}^2$, are also available:

$$\mathcal{B}(\bar{B} \to X_s \ell^+ \ell^-)_{\text{high}} = \begin{cases} \left(0.418 \pm 0.117^{+0.061}_{-0.068}\right) \times 10^{-6} & \text{(Belle)} \\ \left(0.5 \pm 0.25^{+0.08}_{-0.07}\right) \times 10^{-6} & \text{(BaBar)} \\ (0.44 \pm 0.12) \times 10^{-6} & \text{(Average)} \end{cases} \tag{2}$$

By the end of the present B factories an experimental accuracy of 15% is finally expected.

The recently calculated NNLL QCD contributions [5–14] have significantly improved the sensitivity of the inclusive $\bar{B} \to X_s \ell^+ \ell^-$ decay in testing extensions of the SM in the sector

of flavour dynamics, in particular, the value of the dilepton invariant mass q_0^2 for which the differential FBA vanishes is one of the most precise predictions in flavour physics with a theoretical uncertainty of order 5%. This well corresponds to the expected experimental sensitivity of $4-6\%$ at the proposed Super-B factories [15–17].

Also non-perturbative corrections scaling with $1/m_b^2$, $1/m_b^3$, or $1/m_c^2$ [18–24] have to be taken into account. Moreover, factorizable long-distance contributions away from the resonance peaks are important; here using the Krüger-Sehgal approach [25] avoids the problem of double-counting.

In the high-q^2 region, one encounters the breakdown of the heavy-mass expansion at the endpoint; while the partonic contribution vanishes in the end-point, the $1/m_b^2$ and $1/m_b^3$ corrections tend towards a non-zero value. In contrast to the endpoint region of the photon energy spectrum in the $\bar{B} \to X_s\gamma$ decay, no partial all-order resummation into a shape function is possible here. However, for an integrated high-q^2 spectrum an effective expansion is found in inverse powers of $m_b^{\rm eff} = m_b \times (1-\sqrt{\hat{s}_{\rm min}})$ rather than m_b. The expansion converges less rapidly, depending on the lower dilepton mass cut $\hat{s}_{\rm min}$ [11]. Recently it was suggested [24] that the large theoretical uncertainties can be reduced by normalizing the $\bar{B} \to X_s\ell^+\ell^-$ decay rate to the semileptonic $\bar{B} \to X_u\ell\bar{\nu}$ decay rate with the same q^2 cut.

A hadronic invariant-mass cut is imposed in the present experiments (Babar: $m_X < 1.8\,{\rm GeV}$, Belle: $m_X < 2.0\,{\rm GeV}$) in order to eliminate the background such as $b \to c\,(\to se^+\nu)e^-\bar{\nu} = b \to se^+e^- + \text{missing energy}$. The high-dilepton mass region is not affected by this cut, and in the low-dilepton mass region the kinematics with a jet-like X_s and $m_X^2 \le m_b\Lambda_{\rm QCD}$ implies the relevance of the shape function. A recent SCET analysis shows that using the universality of jet and shape functions the $10-30\%$ reduction of the dilepton mass spectrum can be accurately computed using the $\bar{B} \to X_s\gamma$ shape function. Nevertheless effects of subleading shape functions lead to an additional uncertainty of 5% [26, 27].

Finally, as in the $\bar{B} \to X_s\gamma$ case, there are unknown subleading nonperturbative corrections of order $O(\alpha_s\Lambda/m_b)$ which may be estimated by an additional uncertainty of order 5%.

Recently, further refinements were presented such as the NLO QED two-loop corrections to the Wilson coefficients whose size is of order 2% [12]. Furthermore, it was shown that in the QED one-loop corrections to matrix elements large collinear logarithms of the form $\log(m_b^2/m_{\rm lepton}^2)$ survive integration if only a restricted part of the dilepton mass spectrum is considered. This adds another contribution of order $+2\%$ in the low-q^2 region for $\mathcal{B}(\bar{B} \to X_s\mu^+\mu^-)$ [28]. For $\mathcal{B}(\bar{B} \to X_se^+e^-)$, in the current BaBar and Belle setups, the logarithm of the lepton mass gets replaced by angular-cut parameters and the integrated branching ratio for the electrons is expected to be close to that for the muons.

In the present manuscript, we calculate these corrections due to large collinear logarithms also for the dilepton mass spectrum in the high-q^2 window and for the FBA for the first time. In the high-q^2 region these corrections are much larger than in the low-q^2 one; we already anticipate that in the muon channel the former account for -8% of the rate while the latter are only about $+2\%$. We also update the theoretical prediction of the observables using several improvements offered recently in the literature among which the two-loop matrix element of the semileptonic operator P_9 and the $1/m_b^3$ corrections are the most important to date. We present

a new phenomenological analysis of the dilepton mass spectrum in the low- and high-q^2 region and of the FBA. In particular, a new approach to the zero of the FBA is proposed. Moreover, we explore a strategy to reduce the uncertainties due to the $1/m_b$ corrections by normalizing with the semileptonic $\bar{B} \to X_u \ell \bar{\nu}$ decay rate with the same q^2 cut, as was recently proposed in the literature [24]. Finally, we derive model-independent formulae for non-SM values of the high-scale Wilson coefficients.

The present manuscript is organised as follows. In Section 2 we present the master formulae for the calculation of the observables; in particular we discuss the normalization of the branching ratio and forward backward asymmetry and explain the details of the perturbative expansion. In Section 3 we present the novel analytical results on the logarithmically enhanced QED corrections to the forward backward asymmetry and to the decay width in the high-q^2 region and also discuss some nonperturbative subtleties. Furthermore, we analyse the relation of the collinear logarithms and the experimental angular cuts. In Section 4 we present the SM predictions for the branching ratio and forward–backward asymmetry. In Section 5 we draw our conclusions.

2 Master formulae

In this section, we present master formulae for the various observables. We closely follow here the notations of Ref. [28] in order to keep the paper compact. The new results are explicitly derived in the next section.

2.1 Dilepton invariant mass spectrum

Following Ref. [28], the master formula for the $\bar{B} \to X_s \ell^+ \ell^-$ branching ratio reads

$$\frac{\mathrm{d}\mathcal{B}(\bar{B} \to X_s \ell^+ \ell^-)}{\mathrm{d}\hat{s}} = \mathcal{B}(\bar{B} \to X_c e \bar{\nu})_{\rm exp} \left|\frac{V_{ts}^* V_{tb}}{V_{cb}}\right|^2 \frac{4}{C} \frac{\Phi_{\ell\ell}(\hat{s})}{\Phi_u} , \tag{3}$$

where $\hat{s} = q^2/m_{b,\rm pole}$. $\Phi_{\ell\ell}(\hat{s})$ and Φ_u are defined by

$$\frac{\mathrm{d}\Gamma(\bar{B} \to X_s \ell^+ \ell^-)}{\mathrm{d}\hat{s}} = \frac{G_F^2 m_{b,\rm pole}^5}{48\pi^3} |V_{ts}^* V_{tb}|^2 \ \Phi_{\ell\ell}(\hat{s}) , \tag{4}$$

$$\Gamma(\bar{B} \to X_u e \bar{\nu}) = \frac{G_F^2 m_{b,\rm pole}^5}{192\pi^3} |V_{ub}|^2 \ \Phi_u , \tag{5}$$

and we have $\Phi_u = 1 + \mathcal{O}(\alpha_s, \alpha_{\rm em}, \Lambda^2/m_b^2)$. The normalization with the measured semileptonic decay rate minimizes the uncertainty due to the fifth power of m_b; the factor C,

$$C = \left|\frac{V_{ub}}{V_{cb}}\right|^2 \frac{\Gamma(\bar{B} \to X_c e \bar{\nu})}{\Gamma(\bar{B} \to X_u e \bar{\nu})} , \tag{6}$$

is used to avoid spurious uncertainties due to the $b \to X_c e \bar{\nu}$ phase-space factor. This factor can be determined from a global analysis of the semileptonic data [29]. The quantity $\Phi_{\ell\ell}(\hat{s})/\Phi_u$

can be expressed in terms of the low-scale Wilson coefficients and various functions of $\hat{s}$ that arise from the matrix elements. The main formula reads

$$\frac{\Phi_{\ell\ell}(\hat{s})}{\Phi_u} = \sum_{i\le j} \mathrm{Re}\left[C_i^{\mathrm{eff}}(\mu_b)\, C_j^{\mathrm{eff}*}(\mu_b)\, H_{ij}(\mu_b,\hat{s})\right] , \tag{7}$$

where $C_i^{\mathrm{eff}}(\mu_b) \neq C_i(\mu_b)$ only for $i = 7, 8$. The functions $H_{ij}(\mu_b, \hat{s})$ are given in Eq. (116) of Ref. [28] and can be expressed in terms of the coefficients M_i^A listed in Table 6 of Ref. [28], as well as the building blocks S_{99}, S_{77}, S_{79}, and S_{1010} given in Eqs. (112–115) of Ref. [28].

In the low-q^2 region, there are only a few modifications compared to the analysis in Ref. [28]: we update the parametric inputs, the influence of the $c\bar{c}$ resonances are taken into account and the two-loop matrix element of the operator P_9 is given in a more precise way (see Eqs. (48) and (49) of the present paper). The combined effect of these improvements does not change appreciably the central value for the branching ratio obtained in Ref. [28].

In the high-q^2 region, there are several additional changes necessary besides the ones mentioned above. The electromagnetic contributions to the building blocks S_{99}, S_{77}, S_{79}, and S_{1010} are different and are presented here for the first time in Eqs. (40) – (47). $O(1/m_b^3)$ corrections are numerically relevant and explicitly given in Eqs. (6) of Ref. [24]. Finally, the functions F_1^9, F_2^9, F_1^7, F_2^7, F_8^9, and F_8^7 that appear in the coefficients M_i^A (listed in Table 6 of Ref. [28]) are different in the high-q^2 region and are known only numerically. They have been calculated in Ref. [11].[†]

2.1.1 New normalization

The authors of Ref. [24] have shown that it is possible to drastically reduce the size of $1/m_b^2$ and $1/m_b^3$ power corrections to the integrated decay width, by normalizing it to the semileptonic $b \to u\,\ell\,\nu$ rate integrated over the same q^2-interval. This procedure will help reducing the uncertainties induced by the large power corrections to the decay width integrated over the high-s region. The new observable is defined as follows:

$$\mathcal{R}(s_0) = \frac{\displaystyle\int_{\hat{s}_0}^1 \mathrm{d}\hat{s}\, \frac{\mathrm{d}\Gamma(\bar{B}\to X_s\ell^+\ell^-)}{\mathrm{d}\hat{s}}}{\displaystyle\int_{\hat{s}_0}^1 \mathrm{d}\hat{s}\, \frac{\mathrm{d}\Gamma(\bar{B}^0\to X_u\ell\nu)}{\mathrm{d}\hat{s}}} = 4\left|\frac{V_{ts}V_{tb}}{V_{ub}}\right|^2 \frac{\int_{\hat{s}_0}^1 \mathrm{d}\hat{s}\,\Phi_{\ell\ell}(\hat{s})}{\int_{\hat{s}_0}^1 \mathrm{d}\hat{s}\,\Phi_u(\hat{s})} \tag{8}$$

where $\Phi_{\ell\ell}(\hat{s})$ was defined in Eqs. (3) and (4) and the differential $\Phi_u(\hat{s})$ is given by

$$\frac{\mathrm{d}\Gamma_u}{\mathrm{d}\hat{s}} = \frac{G_F^2\,|V_{ub}|^2\, m_{b,\mathrm{pole}}^3}{192\pi^3}\,\Phi_u(\hat{s}) . \tag{9}$$

Explicit expressions for the $O(1, \alpha_s, 1/m_b^2, 1/m_b^3)$ contributions to $\Phi_u(\hat{s})$ can be found in Eqs. (5,11) of Ref. [24]. The $O(\alpha_s^2)$ correction to $\Phi_u(\hat{s})$ is given by $\alpha_s^2 X_2(\hat{s})$ with X_2 defined in Eq. (60) of Ref. [30]. We have not included electromagnetic corrections of order κ in the

[†]Numerical expressions of these functions can be obtained from the authors upon request.

normalization because they are not known. However, the effect of those effects in the conventional approach where the fully integrated semileptonic decay rate is used as normalization is less than 2.5%.

Note that in the definition of $\mathcal{R}$ we used only neutral semileptonic decays in order to reduce the uncertainties coming from weak annihilation contributions ($f_u^0,\ f_u^+,\ f_s^0,\ f_s^+$); in fact, following the analysis of Ref. [31] one concludes that $f_u^0, f_s^0, f_s^+ \ll f_u^+$ (for the definition of the f variables we refer the reader to Ref. [24]).

Obviously, for the comparison of the theoretical ratio $\mathcal{R}$ with experiment, a separate measurement of $B^0 \to X_u \ell \bar{\nu}$ and $B^\pm \to X_u \ell \bar{\nu}$ with a high-q^2 cut is necessary. These are quantities with larger experimental uncertainties. However, they are not expected to negate the drastic reduction of the theoretical uncertainty in the ratio $\mathcal{R}$ (see section 4.2 for numerical results).

2.2 Forward-backward asymmetry

In complete analogy to the formula for the branching ratio, one can derive also a formula that expresses the FBA (see [32]) in terms of the low-scale Wilson coefficients and various building blocks. Normalizing to the semileptonic $B \to X_u e \bar{\nu}$ decay width, we get

$$\frac{\mathrm{d}\mathcal{A}_{FB}(\bar{B} \to X_s \ell^+ \ell^-)}{\mathrm{d}\hat{s}} \;=\; \mathcal{B}(B \to X_c e \bar{\nu})_{\rm exp} \left|\frac{V_{ts}^* V_{tb}}{V_{cb}}\right|^2 \frac{4}{C}\, \frac{\Phi_{\ell\ell}^{FBA}(\hat{s})}{\Phi_u}\,, \tag{10}$$

where $\Phi_{\ell\ell}^{FBA}(\hat{s})$ is defined by ($z = \cos\theta_\ell$)

$$\int_{-1}^{1} \mathrm{d}z\, \mathrm{sgn}(z)\, \frac{\mathrm{d}^2\Gamma(\bar{B} \to X_s \ell^+ \ell^-)}{\mathrm{d}\hat{s}\, \mathrm{d}z} \;=\; \frac{G_F^2 m_{b,\rm pole}^5}{48\pi^3} \left|V_{ts}^* V_{tb}\right|^2\ \Phi_{\ell\ell}^{FBA}(\hat{s})\,, \tag{11}$$

$$\frac{\Phi_{\ell\ell}^{FBA}}{\Phi_u} \;=\; \sum_{i \le j} \mathrm{Re}\left[C_i^{\rm eff}(\mu_b)\ C_j^{\rm eff *}(\mu_b)\ H_{ij}(\mu_b, \hat{s})\right]\,. \tag{12}$$

Again, the functions $H_{ij}(\mu_b, \hat{s})$ depend on the coefficients M_i^A listed in Table 6 of Ref. [28] and on the building blocks S_{710} and S_{910}:

$$H_{ij} = \begin{cases} \sum\limits_{A=7,9} \mathrm{Re}(M_i^A M_i^{10*})\ S_{A10} + \Delta H_{ii}\,, & \text{when } i = j \\ \sum\limits_{A=7,9} \left(M_i^A M_j^{10*} + M_i^{10} M_j^{A*}\right)\ S_{A10} + \Delta H_{ij}\,, & \text{when } i \neq j\,. \end{cases} \tag{13}$$

where S_{710} and S_{910} are given by

$$\begin{aligned} \mathrm{S}_{710} \;=\;& -6\,(1-\hat{s})^2 \Big\{1 + 8\,\widetilde{\alpha}_{\rm s}\,\Big[f_{710}(\hat{s}) + u^{(1)}\Big] + \kappa\, u^{(\rm em)} + 8\,\widetilde{\alpha}_{\rm s}\kappa\,\Big[\omega_{710}^{(\rm em)}(\hat{s}) + u^{(\rm em)}\, f_{710}(\hat{s})\Big] \\ & \qquad +16\,\widetilde{\alpha}_{\rm s}^2\Big[u^{(2)} + 4\,u^{(1)}\, f_{710}(\hat{s})\Big]\Big\} \\ & -\frac{8\,\lambda_1}{m_b^2}\,\hat{s} - \,6\,\frac{\lambda_2}{m_b^2}\,(1 - 14\hat{s} + 9\hat{s}^2)\,, \end{aligned} \tag{14}$$

$$
\begin{aligned}
\mathrm{S}_{910} &= -3\,\hat{s}\,(1-\hat{s})^2\left\{1+8\,\widetilde{\alpha}_{\mathrm{s}}\left[f_{910}(\hat{s})+u^{(1)}\right]+\kappa\,u^{(\mathrm{em})}+8\,\widetilde{\alpha}_{\mathrm{s}}\kappa\,\left[\omega_{910}^{(\mathrm{em})}(\hat{s})+u^{(\mathrm{em})}\,f_{910}(\hat{s})\right]\right. \\
&\qquad \left.+16\,\widetilde{\alpha}_{\mathrm{s}}^2\left[u^{(2)}+4\,u^{(1)}\,f_{910}(\hat{s})\right]\right\} \\
&\quad -\frac{4\,\lambda_1}{m_b^2}\,\hat{s}^2+\frac{12\,\lambda_2}{m_b^2}\,\hat{s}^2\,(4-3\hat{s})\,. \qquad (15)
\end{aligned}
$$

The functions $f_{i10}(\hat{s})$ $(i=7,9)$ can be found in Eqs. (15–17) of Ref. [9]. The functions $\omega_{ij}^{(\mathrm{em})}$ represent the electromagnetic corrections to the matrix elements which are calculated for the first time in the present paper (see Eqs. (32–38)). The S_{AB} also include non-perturbative $\mathcal{O}(1/m_b^2)$ corrections from Refs [19, 22]. Contrary to the expression for the branching ratio the quantity λ_1, which is related to the kinetic energy of the b-quark, does not drop out here. The quantities

$$
\Delta H_{ij} = b_{ij} + c_{ij} + e_{ij} \qquad (16)
$$

have the same meaning as in Eq. (117) of Ref. [28]. They need to be included only for $i=1,2$. The additional $\ln(m_b^2/m_\ell^2)$-enhanced electromagnetic corrections e_{ij} for the FBA read

$$
\begin{aligned}
e_{210} &= -24\,\hat{s}\,(1-\hat{s})^2\,\widetilde{\alpha}_{\mathrm{s}}^2\kappa^2\,\omega_{210}^{(\mathrm{em})}(\hat{s}) \\
e_{110} &= \tfrac{4}{3}e_{210}. \qquad (17)
\end{aligned}
$$

The function $\omega_{210}^{(\mathrm{em})}(\hat{s})$ is again new (see Eq. (34)), while the $\mathcal{O}(\Lambda_{\mathrm{QCD}}^2/m_c^2)$ non-perturbative contributions were calculated in Ref. [21]

$$
\begin{aligned}
c_{210} &= +\widetilde{\alpha}_{\mathrm{s}}\kappa\frac{\lambda_2}{3m_c^2}(1-\hat{s})^2(1+3\hat{s})\,F(r)\,, \\
c_{110} &= -\tfrac{1}{6}\,c_{210}\,, \qquad (18)
\end{aligned}
$$

where $r \equiv 1/y_c = s/(4m_c^2)$ and the function $F(r)$ is listed for example in appendix A of Ref. [28]. The finite bremsstrahlung contributions b_{ij} were calculated in Ref. [13]. We do not present these corrections here but do include them in the numerical analysis.

2.3 Normalization of the FBA

First of all, let us recall that the zero of the FBA is *not* an independent theoretical quantity, thus, it should not be separately expanded in α_s, but its dependence on α_s is fixed by the expansion of the FBA itself.

As discussed in section 2, the normalization of the FBA by the semileptonic decay rate or by the $\bar{B}\to X_s\ell^+\ell^-$ decay rate is important in order to cancel the overall factor $m_{b,\mathrm{pole}}^5$. Moreover, the elimination of renormalon ambiguities requires the analytical conversion to a short-distance mass and the expansion in α_s (see next subsection). If we extract the zero of the FBA without using any normalization, the conversion and the expansion of the overall $m_{b,\mathrm{pole}}^5$ factor induces a large dependence on the scheme we choose for the short distance b mass. In fact, we find a -11% $(+5\%)$ shift in switching from the 1S scheme to the $\overline{\mathrm{MS}}$ (pole) one. This large m_b

scheme dependence can be eliminated only by the complete overall α_s expansion of numerator and denominator by which all conversion factors cancel.

Moreover, it is well-known that the perturbative expansion of the $\bar{B} \to X_s \ell^+ \ell^-$ differential decay rate is not well-behaved and it should not be used as normalization in order not to propagate the corresponding uncertainty into the numerator. It is not surprising that also this procedure leads to a large m_b scheme dependence of the zero: we find a shift of -12% when one compares the 1S to the $\overline{\rm MS}$ scheme.

It is clear, that on theory side we should choose the optimal method to predict the FBA and its zero, in particular we should aim for stable, well-converging perturbative expansions which keep the theoretical errors small. The considerations above led us to propose the following double ratio

$$[\frac{\mathrm{d}\mathcal{A}_{FB}(\bar{B} \to X_s \ell^+ \ell^-)}{\mathrm{d}\hat{s}}] \,/\, [\frac{\mathrm{d}\mathcal{B}(\bar{B} \to X_s \ell^+ \ell^-)}{\mathrm{d}\hat{s}}] \;=\; [\frac{\Phi_{\ell\ell}^{FBA}(\hat{s})}{\Phi_u}] \,/\, [\frac{\Phi_{\ell\ell}(\hat{s})}{\Phi_u}]\,, \tag{19}$$

where the quantities are defined in Eqs. (3) and (10). It is understood that each of the ratios in brackets gets fully expanded in α_s, but no overall expansion is done. Note that each of the two terms multiplied by the experimental semileptonic branching ratio corresponds to an observable.

This represents the optimal quantity to fix the FBA and also its zero for several reasons. The experiments will measure the integrated FBA in two or more bins by constructing $\Delta N/N$ were N is the total number of events and ΔN is the asymmetry between the events in the forward and backward region in either of the bins. Our proposed procedure directly gives the corresponding quantity for the integrated asymmetries, while the Φ_u dependence drops out if we expand the perturbative series sufficiently high. Also the m_b scheme dependence of the zero turns out to be minimal; as we will show in the next section, it is around 1% when we compare 1S, $\overline{\rm MS}$ and pole schemes.

This discussion shows that the estimation of the perturbative error of the zero via the comparison of different normalisations as done in [12] is questionable because the various normalizations are ambiguous and the problem of the large scheme dependence of the b quark mass should be addressed. As we will discuss in section 4.5, the standard analysis of the scale dependence offers a better guidance to the understanding of the perturbative errors in our predictions.

2.4 Perturbative expansion

Some remarks about the perturbative expansion are in order: Large logarithms of the form $\alpha_s \log(m_b/M_W)$ have to be resummed at a given order in perturbation theory using renormalization group techniques. In the case of $b \to s\ell^+\ell^-$, the first large logarithm of the form $\log(m_b/M_W)$ arises already without gluons. Moreover, the amplitude of $b \to s\ell^+\ell^-$ is proportional to $\alpha_{\rm em}$. So naturally we have an expansion in α_s and in $\kappa = \alpha_{\rm em}/\alpha_s$ while resumming all powers of $\alpha_s \log(m_b/M_W)$. The Leading Order (LO) are of order κ, NLO are proportional $\kappa\alpha_s$, NNLO are proportional $\kappa\alpha_s^2$.

It is well-known that this naive α_s expansion is problematic, since the formally-leading $O(1/\alpha_s)$ term in C_9 is accidentally small and much closer in size to an $O(1)$ term. In addition the NLO terms are enhanced by a factor of $m_t^2/(M_W^2 \sin^2\theta_W)$. Therefore, also specific higher order terms in the general $\kappa^n \alpha_s^m$ expansion are numerically important.

The $b \to s\ell^+\ell^-$ decay amplitude has the following structure (up to an overall factor of G_F):

$$\begin{aligned}\mathcal{A} &= \kappa \left[\mathcal{A}_{LO} + \alpha_s\, \mathcal{A}_{NLO} + \alpha_s^2\, \mathcal{A}_{NNLO} + \mathcal{O}(\alpha_s^3)\right] \\ &\quad +\kappa^2 \left[\mathcal{A}_{LO}^{em} + \alpha_s\, \mathcal{A}_{NLO}^{em} + \alpha_s^2\, \mathcal{A}_{NNLO}^{em} + \mathcal{O}(\alpha_s^3)\right] + \mathcal{O}(\kappa^3)\,. \end{aligned} \tag{20}$$

with $\mathcal{A}_{LO} \sim \alpha_s\, \mathcal{A}_{NLO}$ and $\mathcal{A}_{LO}^{em} \sim \alpha_s\, \mathcal{A}_{NLO}^{em}$. All these terms are included in the numerical analysis in a complete manner, together with the appropriate bremsstrahlung corrections, while also the term $\mathcal{A}_{NNLO}$ is practically complete due to the calculations in Refs. [5–14]. The only missing parts originate from the unknown two-loop matrix elements of the QCD-penguin operators whose Wilson coefficients are very small.

Among the contributions to $\mathcal{A}_{NNLO}^{em}$, we include only the terms which are either enhanced by an additional factor of $m_t^2/(M_W^2 \sin^2\theta_W)$ (with respect to $\mathcal{A}_{NLO}^{em}$) [12] or contribute to the $\ln(m_b^2/m_\ell^2)$-enhanced terms at the decay width level. As discussed above, the latter terms were calculated in Ref. [28] for the dilepton mass spectrum in the low-q^2 region, while the corresponding terms for the high-q^2 region and the FBA are calculated for the first time in the present paper.

The perturbative expansion of the ratio $\Phi_{\ell\ell}(\hat{s})/\Phi_u$ has a similar structure to that of the squared amplitude (up to bremsstrahlung corrections and nonperturbative corrections)

$$\begin{aligned}\mathcal{A}^2 &= \kappa^2\Big[\mathcal{A}_{LO}^2 + \alpha_s\, 2\mathcal{A}_{LO}\mathcal{A}_{NLO} + \alpha_s^2\, (\mathcal{A}_{NLO}^2 + 2\mathcal{A}_{LO}\mathcal{A}_{NNLO}) \\ &\qquad +\alpha_s^3\, 2(\mathcal{A}_{NLO}\mathcal{A}_{NNLO} + \ldots) + \mathcal{O}(\alpha_s^4))\Big] \\ &+ \kappa^3\Big[2\mathcal{A}_{LO}\mathcal{A}_{LO}^{em} + \alpha_s\, 2(\mathcal{A}_{NLO}\mathcal{A}_{LO}^{em} + \mathcal{A}_{LO}\mathcal{A}_{NLO}^{em}) \\ &\qquad +\alpha_s^2\, 2(\mathcal{A}_{NLO}\mathcal{A}_{NLO}^{em} + \mathcal{A}_{NNLO}\mathcal{A}_{LO}^{em} + \mathcal{A}_{LO}\mathcal{A}_{NNLO}^{em}) \\ &\qquad +\alpha_s^3\, 2(\mathcal{A}_{NLO}\mathcal{A}_{NNLO}^{em} + \mathcal{A}_{NNLO}\mathcal{A}_{NLO}^{em} + \ldots) + \mathcal{O}(\alpha_s^4)\Big] \\ &+ \mathcal{O}(\kappa^4)\,. \end{aligned} \tag{21}$$

We assume that all products in Eq. (7) are expanded in α_s and κ. Regarding QCD, a strict NNLO calculation of $\Phi_{\ell\ell}(\hat{s})/\Phi_u$ should only include terms up to order $\kappa^2\alpha_s^2$. In the numerical calculation of $\Phi_{\ell\ell}(\hat{s})/\Phi_u$, however, we include all the terms that are written explicitly in Eq. (21). The term $\mathcal{A}_{NLO}\mathcal{A}_{NNLO}$ of order $\kappa^2\alpha_s^3$ is formally a NNNLO term, but numerically important. Within the electromagnetic corrections the same is true for the term $\mathcal{A}_{NLO}^{em}\mathcal{A}_{NNLO}$.

The dots in Eq. (21) stand for the unknown terms $\mathcal{A}_{LO}\mathcal{A}_{NNNLO}$ and $\mathcal{A}_{LO}^{em}\mathcal{A}_{NNNLO}$ and, consequently, can safely be neglected due to $\mathcal{A}_{LO} \sim \alpha_s\mathcal{A}_{NLO}$, $\mathcal{A}_{LO}^{em} \sim \alpha_s\mathcal{A}_{NLO}^{em}$, and $\alpha_s\mathcal{A}_{NNNLO} \ll \mathcal{A}_{NNLO}$. So our calculations almost reach the formal NNNLO QCD accuracy. Those terms beyond the formal NNLO level which are proportional to $|C_7|^2$ and $|C_8|^2$ are scheme independent.

In the following we will therefore call the accuracy of our calculations *improved* NNLO which in fact is very similar to the scheme proposed in Ref. [6] and used in many previous analyses of

the $b \to s\ell^+\ell^-$ observables. In these works the formally-leading, but accidentally small $O(1/\alpha_s)$ term in C_9 is treated as $O(1)$ and absorbed into the NLO coefficient: as consequence the two-loop matrix element of P_9 and the three-loop mixing of the four-quark operators into P_9 are left out even though they are formally NNLO terms. This is the main difference between the NNLO scheme proposed in Ref. [6] and the *improved* NNLO used in the present manuscript.

Finally let us comment on the mass schemes that we use: The pole mass of the b quark appears explicitly in the calculation of the matrix elements ($\hat{s} \equiv s/m^2_{b,\text{pole}}$) and in several loop functions. Unfortunately, the precise determination of the numerical value of $m^2_{b,\text{pole}}$ is hindered by renormalon ambiguities that appear in the relation between any short distance mass definition (e.g. $\overline{\text{MS}}$, 1S, kinetic schemes) and the pole one. We eliminate these renormalon uncertainties utilizing the Upsilon expansion described in Refs. [33, 34]. Every occurrence of the pole mass is converted analytically to the $1S$-mass before any numerical evaluation of the branching ratio is performed. In our analysis we use the conversion formula up to order α_s^2 [34]. We follow a similar approach for the treatment of the charm pole mass that appears in the calculation of some matrix elements. We adopt the $\overline{\text{MS}}$ charm mass as input and expand the pole mass at order α_s^2 using the formulae presented in Ref. [34]. For what concerns the top mass, we take the pole mass as input and convert it to the $\overline{\text{MS}}$ scheme at order α_s^3. The perturbative expansion of the FBA proceeds along the same lines.

3 Analytical results

In this section, we calculate the electromagnetic corrections to the matrix elements for the FBA in the low- and high-q^2 region and for the dilepton mass spectrum in the high-q^2 region. Moreover, we present a more precise fixing of the two-loop matrix elements of the P_9 operator. Finally, we make some remarks on some non–perturbative subtleties.

3.1 Log-enhanced corrections to the FBA, low- and high-q^2 region

First we derive the basic formulae to obtain the expressions for the $\ln(m_b^2/m_\ell^2)$-enhanced corrections to the FBA, where we shall focus here on the un-normalized asymmetry[‡] corresponding to the LHS of Eq. (11). We follow closely the notation of Section 5 of Ref. [28].

It was shown in the Appendix of Ref. [19] that the angular FBA with respect to θ_ℓ, the angle in the dilepton c.m.s. between the directions of the momenta of the decaying $\bar{B}$ and the positively charged lepton, is equivalent to the energy asymmetry between the two leptons in the rest–frame of the decaying $\bar{B}$. Events in which $\cos\theta_\ell > 0$ in the dilepton c.m.s. correspond to events in which $E_- > E_+$ measured in the $\bar{B}$-meson restframe, where $E_\pm$ denotes the $\ell^\pm$-energy. Sticking to the latter frame and defining the scaled energies

$$y_\pm \equiv \frac{2\,E_\pm}{m_b}\,, \tag{22}$$

[‡]In this subsection we suppress the normalization factor, thus, the symbol $\mathcal{A}_{FB}$ denotes the un-normalized FBA, see Eqs. (23), (27), and (31).

we can write the fully differential FBA as

$$d\mathcal{A}_{FB} = PF\; d\hat{s}\; dy_+\; dy_-\; \delta(1+\hat{s}-y_+-y_-)\; |\mathcal{A}|^2\; \mathrm{sgn}(y_- - y_+), \tag{23}$$

with the pre-factor

$$PF = \frac{G_F^2 m_b |V_{tb}V_{ts}^*|^2}{32\pi^3}\; . \tag{24}$$

We are mainly interested in $\ln(m_b^2/m_\ell^2)$-enhanced electromagnetic corrections. They are derived by means of the splitting function and we shall adopt the kinematics from Figure 2 of Ref. [28]. In the collinear limit the fully differential FBA reads

$$d\mathcal{A}_{FB,\mathrm{coll}}^{(m)} = PF\; dx\; d\hat{s}\; dy_+\; dy_-\; \delta(1+\hat{s}-y_+-y_-)\, f_\gamma^{(m)}(x)\; |\mathcal{A}|^2\; \mathrm{sgn}(y_- - y_+)\; . \tag{25}$$

We shall only retain the $\ln(m_b^2/m_\ell^2)$-enhanced part of $f_\gamma^{(m)}$, which then becomes independent of E,

$$f_\gamma^{(m)}(x) = 4\,\tilde{\alpha}_e\, \frac{[1+(1-x)^2]}{x}\, \ln\!\left(\frac{m_b}{m_\ell}\right)\; . \tag{26}$$

In the squared amplitude in Eq. (25) we keep only those terms that are relevant for the FBA, i. e. all terms that do not drop out upon integration over the sign-function,

$$\begin{aligned} |\mathcal{A}|^2 \;&=\; 2\,\mathrm{Re}\Big[C_{10}C_9^* + \tilde{\alpha}_s\kappa\; C_{10}(C_2 + C_F\; C_1) f_2^*(\hat{s})\Big]\; \langle P_{10}\rangle_{\mathrm{tree}} \langle P_9\rangle_{\mathrm{tree}}^* \\ &\quad +2\;\mathrm{Re}[C_{10}C_7^*]\; \langle P_{10}\rangle_{\mathrm{tree}} \langle P_7\rangle_{\mathrm{tree}}^*\; . \end{aligned} \tag{27}$$

As in the case of the decay width we must consider the difference

$$\frac{d\mathcal{A}_{FB,\mathrm{coll},2}^{(m)}}{d\hat{s}} - \frac{d\mathcal{A}_{FB,\mathrm{coll},3}^{(m)}}{d\hat{s}}\; , \tag{28}$$

where we stay differential in the double and in the triple invariant, respectively. At this point more care is required compared to the calculation of the decay width. Due to the emergence of the sign-function in Eq. (25) we must distinguish between photon-emission from the ℓ^+ and from the ℓ^- in case of the double invariant. In the former case we have to stay differential in $\hat{s} = (\bar{x}p_1 + p_2)^2/m_b^2$, in the latter in $\hat{s} = (p_1 + \bar{x}p_2)^2/m_b^2$. Also the $y_\pm$ change accordingly. We therefore have

$$\begin{aligned} \frac{d\mathcal{A}_{FB,\mathrm{coll},2,\ell^\pm}^{(m)}}{d\hat{s}} \;&=\; \pm PF \left[\int_0^{1-\sqrt{\hat{s}}} dx \int_{\hat{s}/\bar{x}}^{\frac{\bar{x}+\hat{s}}{\bar{x}(1+\bar{x})}} dy_\pm + \int_{1-\sqrt{\hat{s}}}^{1-\hat{s}} dx \int_{\hat{s}/\bar{x}}^{1} dy_\pm - \int_0^{1-\sqrt{\hat{s}}} dx \int_{\frac{\bar{x}+\hat{s}}{\bar{x}(1+\bar{x})}}^{1} dy_\pm \right] \\ &\quad \times \frac{f_\gamma^{(m)}(x)}{\bar{x}}\; |\mathcal{A}|^2\; \big|_{\hat{s}\to\hat{s}/\bar{x}\;;\; y_\mp \to 1-y_\pm+\hat{s}/\bar{x}} \quad . \end{aligned} \tag{29}$$

The two expressions corresponding to upper and lower sign should be equal due to the antisymmetry of $|\mathcal{A}|^2$ in $y_+ \leftrightarrow y_-$. The case of the triple invariant is simpler since we stay differential

in $\hat{s} = (p_1 + p_2)^2/m_b^2$, namely

$$\frac{d\mathcal{A}_{FB,\mathrm{coll},3,\ell^\pm}^{(m)}}{d\hat{s}} = \pm PF \int_0^1 dx \left[\int_{\hat{s}}^{\frac{1+\hat{s}}{2}} dy_\pm - \int_{\frac{1+\hat{s}}{2}}^{1} dy_\pm \right] f_\gamma^{(m)}(x)\ |\mathcal{A}|^2 \,|_{\,y_\mp \to 1 - y_\pm + \hat{s}} \quad , \tag{30}$$

where the expression for the upper and lower sign should again be equal due to the antisymmetry of $|\mathcal{A}|^2$. We finally have to combine the expressions according to Eq. (28).

The corrections to the unnormalized FBA read

$$\begin{aligned}
\frac{\mathrm{d}\Delta\mathcal{A}_{FB}}{d\hat{s}} &= \frac{G_F^2 m_b^5}{48\pi^3} |V_{ts}^* V_{tb}|^2\ \Delta\Phi_{\ell\ell}^{FBA}(\hat{s}) \\
&= \frac{G_F^2 m_b^5}{48\pi^3} |V_{tb} V_{ts}^*|^2 (1-\hat{s})^2 \widetilde{\alpha}_\mathrm{s}\kappa \Bigg\{ -48 \left[\widetilde{\alpha}_\mathrm{s}\kappa\, \mathrm{Re}\left[C_7 C_{10}^*\right]\ \omega_{710}^{(\mathrm{em})}(\hat{s}) \right] \\
&\quad -24\,\hat{s} \left[\mathrm{Re}\left[C_9 C_{10}^*\right]\ \omega_{910}^{(\mathrm{em})}(\hat{s}) + \widetilde{\alpha}_\mathrm{s}\kappa\ \mathrm{Re}\left[(C_2 + C_F C_1) C_{10}^*\, \omega_{210}^{(\mathrm{em})}(\hat{s}) \right] \right] \Bigg\} \quad , \qquad (31)
\end{aligned}$$

with

$$\omega_{710}^{(\mathrm{em})}(\hat{s}) = \ln\left(\frac{m_b^2}{m_\ell^2}\right) \left[\frac{7 - 16\sqrt{\hat{s}} + 9\,\hat{s}}{4\ (1-\hat{s})} + \ln(1-\sqrt{\hat{s}}) + \frac{1+3\,\hat{s}}{1-\hat{s}}\ \ln\left(\frac{1+\sqrt{\hat{s}}}{2}\right) - \frac{\hat{s}\ \ln\hat{s}}{(1-\hat{s})} \right] , \tag{32}$$

$$\begin{aligned}
\omega_{910}^{(\mathrm{em})}(\hat{s}) &= \ln\left(\frac{m_b^2}{m_\ell^2}\right) \left[-\frac{5 - 16\sqrt{\hat{s}} + 11\,\hat{s}}{4\ (1-\hat{s})} + \ln(1-\sqrt{\hat{s}}) \right. \\
&\quad \left. + \frac{1-5\,\hat{s}}{1-\hat{s}}\ \ln\left(\frac{1+\sqrt{\hat{s}}}{2}\right) - \frac{(1-3\,\hat{s})\ \ln\hat{s}}{(1-\hat{s})} \right] , \qquad (33)
\end{aligned}$$

$$\omega_{210}^{(\mathrm{em})}(\hat{s}) = \ln\left(\frac{m_b^2}{m_\ell^2}\right) \left[-\frac{\Sigma_7(\hat{s}) + i\,\Sigma_7^I(\hat{s})}{24\,\hat{s}\,(1-\hat{s})^2} \right] + \frac{8}{9}\,\omega_{910}^{(\mathrm{em})}(\hat{s})\ \ln\left(\frac{\mu_b}{5\mathrm{GeV}}\right) \ . \tag{34}$$

The functions $\omega_{710}^{(\mathrm{em})}(\hat{s})$ and $\omega_{910}^{(\mathrm{em})}(\hat{s})$ are known in the entire q^2-region, whereas the function $\omega_{210}^{(\mathrm{em})}(\hat{s})$ was obtained by a least squares fit. The function Σ_7, valid in the low-$\hat{s}$-region, reads

$$\Sigma_7(\hat{s}) = -0.259023 - 28.424\,\hat{s} + 205.533\,\hat{s}^2 - 603.219\,\hat{s}^3 + 722.031\,\hat{s}^4 \ , \tag{35}$$

$$\Sigma_7^I(\hat{s}) = \left[-12.20658 - 215.8208\,(\hat{s}-a) + 412.1207\,(\hat{s}-a)^2 \right] (\hat{s}-a)^2\,\theta(\hat{s}-a) \ , \tag{36}$$

with $a = (4m_c^2/m_b^2)^2$. In the high-$\hat{s}$-region the function Σ_7 reads ($\delta = 1 - \hat{s}$)

$$\Sigma_7(\hat{s}) = 77.0256\,\delta^2 - 264.705\,\delta^3 + 595.814\,\delta^4 - 610.1637\,\delta^5 \ , \tag{37}$$

$$\Sigma_7^I(\hat{s}) = 135.858\,\delta^2 - 618.990\,\delta^3 + 1325.040\,\delta^4 - 1277.170\,\delta^5 \ . \tag{38}$$

The polynomials in the high-$\hat{s}$-region were obtained such as to have a double zero at $\hat{s} = 1$.

3.2 Log-enhanced corrections to the BR, high-q^2 region

The log-enhanced corrections to the differential decay width given in Eq. (4) read

$$\begin{aligned}\frac{\mathrm{d}\Delta\Gamma}{d\hat{s}} &= \frac{G_F^2 m_b^5}{48\pi^3}|V_{tb}V_{ts}^*|^2(1-\hat{s})^2\widetilde{\alpha}_\mathrm{s}\kappa\Bigg\{8\,(1+2\hat{s})\Bigg[|C_9|^2\;\omega_{99}^{(\mathrm{em})}(\hat{s})+|C_{10}|^2\;\omega_{1010}^{(\mathrm{em})}(\hat{s})\\ &+\widetilde{\alpha}_\mathrm{s}\kappa\;\mathrm{Re}\Big[(C_2+C_FC_1)C_9^*\;\omega_{29}^{(\mathrm{em})}(\hat{s})\Big]+\widetilde{\alpha}_\mathrm{s}^2\kappa^2\;(C_2+C_FC_1)^2\;\omega_{22}^{(\mathrm{em})}(\hat{s})\Bigg]\\ &+96\left[\widetilde{\alpha}_\mathrm{s}\kappa\;\mathrm{Re}\,[C_7C_9^*]\;\omega_{79}^{(\mathrm{em})}(\hat{s})+\widetilde{\alpha}_\mathrm{s}^2\kappa^2\;\mathrm{Re}\Big[(C_2+C_FC_1)C_7^*\;\omega_{27}^{(\mathrm{em})}(\hat{s})\Big]\right]\\ &+8\,(4+\frac{8}{\hat{s}})\widetilde{\alpha}_\mathrm{s}^2\kappa^2\;|C_7|^2\;\omega_{77}^{(\mathrm{em})}(\hat{s})\Bigg\}\;. \end{aligned} \tag{39}$$

Exact analytical expressions are known for the functions $\omega_{99}^{(\mathrm{em})}(\hat{s})$, $\omega_{1010}^{(\mathrm{em})}(\hat{s})$, $\omega_{77}^{(\mathrm{em})}(\hat{s})$, and $\omega_{79}^{(\mathrm{em})}(\hat{s})$ (see Eqs. (94) and (100) – (102) of Ref. [28]). Therefore, they hold in the entire q^2-region, while the other ω-functions are obtained by a least-squares fit in the high-q^2-region (for fixed values of m_b and m_c):

$$\omega_{29}^{(\mathrm{em})}(\hat{s}) = \ln\left(\frac{m_b^2}{m_\ell^2}\right)\left[\frac{\Sigma_4(\hat{s})+i\,\Sigma_4^I(\hat{s})}{8(1-\hat{s})^2(1+2\hat{s})}\right]+\frac{16}{9}\,\omega_{1010}^{(\mathrm{em})}(\hat{s})\;\ln\Big(\frac{\mu_b}{5\mathrm{GeV}}\Big)\;, \tag{40}$$

$$\begin{aligned}\omega_{22}^{(\mathrm{em})}(\hat{s}) &= \ln\left(\frac{m_b^2}{m_\ell^2}\right)\left[\frac{\Sigma_5(\hat{s})}{8(1-\hat{s})^2(1+2\hat{s})}+\frac{\Sigma_4(\hat{s})}{9(1-\hat{s})^2(1+2\hat{s})}\ln\Big(\frac{\mu_b}{5\mathrm{GeV}}\Big)\right]\\ &+\frac{64}{81}\;\omega_{1010}^{(\mathrm{em})}(\hat{s})\;\ln^2\Big(\frac{\mu_b}{5\mathrm{GeV}}\Big)\;,\end{aligned} \tag{41}$$

$$\omega_{27}^{(\mathrm{em})}(\hat{s}) = \ln\left(\frac{m_b^2}{m_\ell^2}\right)\left[\frac{\Sigma_6(\hat{s})+i\,\Sigma_6^I(\hat{s})}{96(1-\hat{s})^2}\right]+\frac{8}{9}\,\omega_{79}^{(\mathrm{em})}(\hat{s})\;\ln\Big(\frac{\mu_b}{5\mathrm{GeV}}\Big)\;, \tag{42}$$

with the functions Σ_i, valid in the high-$\hat{s}$-region ($\delta = 1-\hat{s}$):

$$\Sigma_4(\hat{s}) = -148.061\,\delta^2+492.539\,\delta^3-1163.847\,\delta^4+1189.528\,\delta^5\;, \tag{43}$$

$$\Sigma_4^I(\hat{s}) = -261.287\,\delta^2+1170.856\,\delta^3-2546.948\,\delta^4+2540.023\,\delta^5\;, \tag{44}$$

$$\Sigma_5(\hat{s}) = -221.904\,\delta^2+900.822\,\delta^3-2031.620\,\delta^4+1984.303\,\delta^5\;, \tag{45}$$

$$\Sigma_6(\hat{s}) = -298.730\,\delta^2+828.0675\,\delta^3-2217.6355\,\delta^4+2241.792\,\delta^5\;, \tag{46}$$

$$\Sigma_6^I(\hat{s}) = -528.759\,\delta^2+2095.723\,\delta^3-4681.843\,\delta^4+5036.677\,\delta^5\;. \tag{47}$$

The fits are excellent for $\hat{s} > 0.65$. Again, the polynomials were obtained such as to have a double zero at $\hat{s} = 1$.

3.3 Two-loop matrixelement of P_9

In Ref. [12], an estimate of the two-loop (NNLO) matrix element of the operator P_9 – denoted $\omega_{99}^{(2)}(\hat{s})$ in Eq. (74) of Ref. [28] – was presented which was neglected in all previous analyses. The

estimate is based on the fact that the QCD corrections to $b \to s\ell^+\ell^-$ are identical to those of $b \to u\ell\nu$ ($t \to b\ell\nu$), in the limit of vanishing strange (bottom) quark mass. However, the specific two-loop calculation of the $b \to u\ell\nu$ decay was available as an expansion in $(1-\hat{s})$ [35], while the two-loop contribution of the top quark decay was only known as an expansion of M_W^2/m_t^2 (which translates into an expansion in q^2/m_b^2 for $b \to s\ell\ell$) up to the second order based on Pade approximation methods [36]. In the meanwhile, the QCD corrections to $b \to u\ell\nu$ are also known as an expansion in $\hat{s}$ [30, 37].

Thus, in the low-$\hat{s}$ region we approximate the function $\omega_{99}^{(2)}$ by the in $\hat{s} = \omega$ expanded results

$$\omega_{99}^{(2)}(\hat{s}) \equiv X_2(\omega = \hat{s})/X_0(\omega = \hat{s}) \tag{48}$$

where $X_2(\omega)$ is given in Eq. (60) of Ref. [30] and $X_0(\omega)$ in Eq. (2) of Ref [37].

Analogously, in the high-$\hat{s}$ region we approximate the function $\omega_{99}^{(2)}$ by the in $(1-\hat{s}) = \delta$ expanded results of $X_2(\delta = 1-\hat{s})$ and $X_0(\delta = 1-\hat{s})$ as given in Eq. (2) and (3) of Ref. [35]. Note that the normalization of the X_i differs by a factor of 2 in Ref. [35] and Refs. [30, 37].[§]

3.4 Some nonperturbative subleties

For a detailed discussion of nonperturbative corrections we refer the reader to Section 5 of Ref. [11]. Here we add few remarks on some specific issues.

The long-distance corrections related to the $c\bar{c}$ intermediate states originate from the nonperturbative interactions of the $c\bar{c}$ pair in the process $\bar{B} \to X_s c\bar{c} \to X_s \ell^+\ell^-$. If the dilepton invariant mass is near the first two $J^{PC} = 1^{--}$ $c\bar{c}$ resonances (Ψ and Ψ'), this effect is very large and shows up as a peak in the dilepton mass spectrum which can easily be eliminated by suitable kinematical cuts. More delicate is the estimate of such long-distance effects away from the resonance peaks in the perturbative windows.

Within the KS–approach [25], one reabsorbs charm rescattering effects into the matrix element of P_9; the effects of $b \to c\bar{c}s$ operators is estimated by means of experimental data on $\sigma(e^+e^- \to c\bar{c}$ hadrons) using a dispersion relation. To be more specific, the function $h(z,s)$ appearing in Eq. (A.5) of Ref. [11] (which corresponds to the expression $g(y_c) + 8/9\log(m_b/m_c) - 4/9$ in Eq. (72) of Ref. [28]) is replaced by ($z = m_c^2/m_b^2$)

$$h(z,\hat{s}) \longrightarrow h(z,0) + \frac{s}{3} P \int_{m_\pi^2}^{\infty} d\hat{s}' \frac{R_{\rm had}^{c\bar{c}}(\hat{s}')}{\hat{s}'(\hat{s}'-\hat{s})} + i\frac{\pi}{3} R_{\rm had}^{c\bar{c}}(\hat{s}) \ , \tag{49}$$

where $R_{\rm had}^{c\bar{c}}(\hat{s}) = \sigma(e^+e^- \to c\bar{c})/\sigma(e^+e^- \to \mu^+\mu^-)$. This method is exact only in the limit in which the $\bar{B} \to X_s c\bar{c}$ transition can be factorized into the product of $\bar{s}b$ and $\bar{c}c$ colour-singlet currents. It is possible to take into account non-factorizable effects and reproduce the correct hadronic branching ratios by multiplying $R_{\rm had}^{c\bar{c}}$ by a purely phenomenological factor $\kappa = 2.6$. However, a model-independent way to estimate the non-factorizable $c\bar{c}$ long-distance effects far from the resonance region exists by means of an expansion in inverse powers of the charm-quark mass [20, 21]. Having included those $1/m_c$ corrections, an 'inflation' of the factorizable

[§]There is a typo in Eq. (4) of Ref. [35]: the powers of the last four δ's have to be increased by 1 each.

KS-corrections using the phenomenological factor κ would lead to a *double-counting*. The numerical impact of the KS contribution to the integrated rate in the low- and high-s regions is about $+2\%$ and -10%, respectively.

In Section 5 of Ref. [11], another large nonperturbative error for the high-q^2 region was located in the *linear* $1/m_b$ corrections. The physical observables defined in terms of a q^2-cut are sensitive to a $1/m_b$ term via the the uncertainty on the value of $m_{b,\rm pole}$ or equivalently via the relation of the pole mass and the hadron mass

$$M_B = m_b(1 + \bar{\Lambda}/m_b + O(1/m_b^2)). \tag{50}$$

Choosing as reference cut the value $\hat{s}_{\rm min} = 0.6$, the integrated normalized dilepton mass spectrum defined in terms of $q^2_{\rm min}$ can be written as

$$\begin{aligned} R_{\rm cut}(q^2_{\rm min}) &= \int_{q^2>q^2_{\rm min}} dq^2 \frac{d\Gamma(\bar{B}\to X_s\ell^+\ell^-)}{\Gamma(\bar{B}\to X_c e\nu)} \\ &= \left\{1 - 6.2\left(\frac{q^2_{\rm min}}{m_b^2} - 0.6\right) + O\left[\left(\frac{q^2_{\rm min}}{m_b^2} - 0.6\right)^2\right]\right\} \times \int_{0.6}^1 ds\ R(s)\ , \end{aligned} \tag{51}$$

which implies

$$\frac{\delta R_{\rm cut}}{R_{\rm cut}} \approx 7.4 \frac{\delta m_b}{m_b}\ . \tag{52}$$

Using the pole mass scheme with $\delta m_b = 0.1$ GeV, this leads to a $\approx 15\%$ error on $R_{\rm cut}$. However, this error gets now significantly reduced in our updated analysis using the kinematical 1S scheme for the m_b mass.

3.5 Collinear logarithm in the ee and $\mu\mu$ final state

After inclusion of the NLO QED matrix elements the electron and muon channels receive different contributions due to terms involving $\ln(m_b^2/m_\ell^2)$. As already pointed out in Ref. [28], the presence of this logarithm is strictly related to the definition of the dilepton invariant mass. The collinear logarithm $\ln(m_b^2/m_\ell^2)$ disappears if all photons emitted by the final state on-shell leptons are included in the definition of q^2: $(p_{\ell_1} + p_{\ell_2})^2 \to (p_{\ell_1} + p_{\ell_2} + p_\gamma)^2$. If none of these photons was included in the definition of q^2 – i. e. if a perfect separation of leptons and collinear photons was possible experimentally – then our expressions containing $\ln(m_b^2/m_\ell^2)$ were directly applicable. This is the case for muons since the separation of muons and collinear photons is practically perfect [44]. For electrons with the current Babar and Belle setups the lepton mass gets replaced by an effective mass parameter Λ which is found to be of the same order as m_μ. Hence our numerical results in section 4 for muonic final states should be applied also to the case of electronic final states in the present Babar and Belle setups. All results in section 4 for the electron channel are given under the assumptions of perfect separation of electrons and collinear photons. We refer the reader to section 6 of Ref. [28] for more details.

$\alpha_s(M_z) = 0.1189 \pm 0.0010$ [38]	$m_e = 0.51099892$ MeV
$\alpha_e(M_z) = 1/127.918$	$m_\mu = 105.658369$ MeV
$s^2_W \equiv \sin^2\theta_W = 0.2312$	$m_\tau = 1.77699$ GeV
$\lvert V_{ts}V_{tb}/V_{cb}\rvert^2 = 0.962 \pm 0.002$ [39]	$m_c(m_c) = (1.224 \pm 0.017 \pm 0.054)$ GeV [40]
$\lvert V_{ts}V_{tb}/V_{ub}\rvert^2 = (1.28 \pm 0.12) \times 10^2$ [39]	$m_b^{1S} = (4.68 \pm 0.03)$ GeV [29]
$BR(B \to X_c e\bar{\nu})_{\rm exp} = 0.1061 \pm 0.0017$ [41]	$m_{t,\rm pole} = (170.9 \pm 1.8)$ GeV [42]
$M_Z = 91.1876$ GeV	$m_B = 5.2794$ GeV
$M_W = 80.426$ GeV	$C = 0.58 \pm 0.01$ [29]
$\lambda_2^{\rm eff} = (0.12 \pm 0.02)$ GeV^2	$\rho_1 = (0.06 \pm 0.06)$ GeV^3 [29]
$\lambda_1^{\rm eff} = (-0.243 \pm 0.055)$ GeV^2 [40]	$f_u^0 + f_s = (0 \pm 0.2)$ GeV^3 [24]
$f_u^0 - f_s = (0 \pm 0.04)$ GeV^3 [24]	$f_u^\pm = (0 \pm 0.4)$ GeV^3 [24]

Table 1: Numerical inputs that we use in the phenomenological analysis. Unless explicitly specified, they are taken from PDG 2004 [43].

4 Numerical results

The numerical inputs that we adopt are summarized in Table 1.

4.1 Branching ratio in the high-q^2 region

For the branching ratio integrated over the region $q^2 > 14.4$ GeV^2 we find:

$$\begin{aligned}
\mathcal{B}^{\rm high}_{\mu\mu} &= 2.40 \times 10^{-7} \Big(1 + \left[{}^{+0.01}_{-0.02}\right]_{\mu_0} + \left[{}^{+0.14}_{-0.06}\right]_{\mu_b} \pm 0.02_{m_t} + \left[{}^{+0.006}_{-0.003}\right]_{C,m_c} \pm 0.05_{m_b} + \left[{}^{+0.0002}_{-0.001}\right]_{\alpha_s} \\
&\quad \pm 0.002_{\rm CKM} \pm 0.02_{{\rm BR}_{sl}} \pm 0.05_{\lambda_2} \pm 0.19_{\rho_1} \pm 0.14_{f_s} \pm 0.02_{f_u}\Big) \\
&= 2.40 \times 10^{-7} \, (1^{+0.29}_{-0.26}) \,, \qquad (53) \\
\mathcal{B}^{\rm high}_{ee} &= 2.09 \times 10^{-7} \Big(1 + \left[{}^{+0.02}_{-0.04}\right]_{\mu_0} + \left[{}^{+0.16}_{-0.08}\right]_{\mu_b} \pm 0.02_{m_t} + \left[{}^{+0.005}_{-0.0009}\right]_{C,m_c} \pm 0.05_{m_b} + \left[{}^{+0.0003}_{-0.002}\right]_{\alpha_s} \\
&\quad \pm 0.002_{\rm CKM} \pm 0.02_{{\rm BR}_{sl}} \pm 0.05_{\lambda_2} \pm 0.22_{\rho_1} \pm 0.16_{f_s} \pm 0.02_{f_u}\Big) \\
&= 2.09 \times 10^{-7} \, (1^{+0.32}_{-0.30}) \,. \qquad (54)
\end{aligned}$$

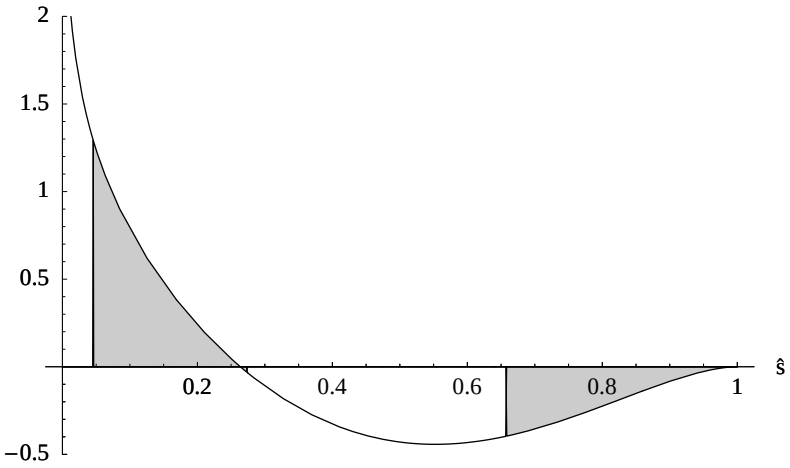

Figure 1: The log–enhanced part of $(1-\hat{s})^2(1+2\hat{s})\,\omega_{99}^{(\mathrm{em})}(\hat{s})$, see Eq. (94) of Ref. [28]. This function integrates to zero, but gives contributions of opposite sign to the low-$\hat{s}$ and high-$\hat{s}$ branching ratio, respectively (shaded areas). The moduli of the absolute shifts are of comparable size. However, the relative effect is much larger in the high-$\hat{s}$ compared to the low-$\hat{s}$ region due to the steep decrease of the differential decay width at large $\hat{s}$.

The scale uncertainty has been estimated by varying the matching scale μ_0 and the low-energy scale μ_b by factors of 2 around their central values (120 and 5 GeV, respectively). In our approach we normalized the $b \to s\ell\ell$ decay width to the semileptonic rate averaged over neutral and charged B mesons; hence, we average f_u^0 and $f_u^\pm$. From the values quoted in Table 1 we obtain: $f_u = 0 \pm 0.2$ and $f_s = 0 \pm 0.1$. The other parametric uncertainties are obtained by varying the inputs within the errors given in Table 1. We assume the errors on C and m_c to be fully correlated. The total error is obtained by adding the individual uncertainties in quadrature. We note that here and in the following all errors are parametric and perturbative uncertainties only and that subleading nonperturbative corrections of order $O(\alpha_s\Lambda/m_b)$ will give an additional uncertainty.

Log–enhanced QED bremsstrahlung corrections shift the central value by about -8% and -20% for the muonic and the electronic final state, respectively. These relative shifts are much larger than the corresponding ones in the low-q^2 region. In fact, these corrections vanish when integrated over the whole dilepton invariant mass spectrum, but are relevant if one is restricted to certain regions in phase space. One observes that the absolute shifts in the central values of the branching ratio are of similar size but of opposite sign in the low-q^2 compared to the high-q^2 region, namely for the muonic final state $+3\times10^{-8}$ and -2×10^{-8} respectively. But since the differential decay width decreases steeply at large q^2, the relative effect is much more pronounced in the high-q^2 compared to the low-q^2 region. See also Fig. 1 for illustration.

4.2 Ratio $\mathcal{R}(s_0)$

The numerical results we obtain for the ratio $\mathcal{R}(s_0)$ discussed in Section 2.1.1 are for $s_0 = 14.4$ GeV^2:

$$\begin{aligned}
\mathcal{R}(s_0)^{\text{high}}_{\mu\mu} &= 2.29 \times 10^{-3}\Big(1 \pm 0.04_{\text{scale}} \pm 0.02_{m_t} \pm 0.01_{C,m_c} \pm 0.006_{m_b} \pm 0.005_{\alpha_s} \pm 0.09_{\text{CKM}} \\
&\quad \pm 0.003_{\lambda_2} \pm 0.05_{\rho_1} \pm 0.03_{f_u^0+f_s} \pm 0.05_{f_u^0-f_s}\Big) \\
&= 2.29 \times 10^{-3}(1 \pm 0.13)\,, \qquad (55) \\
\mathcal{R}(s_0)^{\text{high}}_{ee} &= 1.94 \times 10^{-3}\Big(1 \pm 0.06_{\text{scale}} \pm 0.02_{m_t} \pm 0.02_{C,m_c} \pm 0.004_{m_b} \pm 0.006_{\alpha_s} \pm 0.09_{\text{CKM}} \\
&\quad \pm 0.01_{\lambda_2} \pm 0.09_{\rho_1} \pm 0.05_{f_u^0+f_s} \pm 0.05_{f_u^0-f_s}\Big) \\
&= 1.94 \times 10^{-3}(1 \pm 0.16)\,. \qquad (56)
\end{aligned}$$

Note that uncertainties from poorly known $O(1/m_b^3)$ power corrections are now under control; the largest source of error is V_{ub}.

4.3 Branching ratio in the low-q^2 region

For the branching ratio integrated in the range 1 GeV$^2 < m_{\ell\ell}^2 < 6$ GeV^2 it was found in Ref. [28]:

$$\begin{aligned}
\mathcal{B}_{\mu\mu} &= \Big[1.59 \pm 0.08_{\text{scale}} \pm 0.06_{m_t} \pm 0.024_{C,m_c} \pm 0.015_{m_b} \\
&\quad \pm 0.02_{\alpha_s(M_Z)} \pm 0.015_{\text{CKM}} \pm 0.026_{\text{BR}_{sl}}\Big] \times 10^{-6} = (1.59 \pm 0.11) \times 10^{-6}\,, \qquad (57) \\
\mathcal{B}_{ee} &= \Big[1.64 \pm 0.08_{\text{scale}} \pm 0.06_{m_t} \pm 0.025_{C,m_c} \pm 0.015_{m_b} \\
&\quad \pm 0.02_{\alpha_s(M_Z)} \pm 0.015_{\text{CKM}} \pm 0.026_{\text{BR}_{sl}}\Big] \times 10^{-6} = (1.64 \pm 0.11) \times 10^{-6}\,. \qquad (58)
\end{aligned}$$

We note that we find for $\mathcal{B}_{\mu\mu}$ a $+1.8\%$ shift of the central value due to the KS-corrections which were discussed in Section 3.4 and which were not included in the previous analysis. Moreover, the update of the input parameters (CKM, m_t, α_s) leads to a -3.1% shift; thus, we end up to an overall change of -1.3% within our new phenomenolgical analysis compared with the previous one in Ref. [28]. The total error, being from parametric and perturbative uncertainties only, remains unchanged.

4.4 Integrated FBA in low-s region

By the end of the current B factories the fully differential FBA will not be accessible experimentally, contrary to the integral over one or more bins in the low-q^2 region. However, these integrals can already serve of gain important information on the shape of the FBA and to constrain the parameter space of new physics models (see for instance [45]). We now give the results for the integrated FBA based on Eq. (19). We subdivide the low-$\hat{s}$ region into the two bins $s \in [1, 3.5]$ GeV^2 and $s \in [3.5, 6]$ GeV^2, which we will call bin 1 and bin 2, respectively¶.

¶Predictions for different bins can be produced upon request.

We then integrate the numerator of the double ratio, Eq. (10), over the respective bin, and divide the result by the denominator of the double ratio, Eq. (3) integrated over the same bin, i. e. we first integrate FBA and branching ratio separately and subsequently divide the two numbers. Our results read:

$$\begin{aligned}
\left(\bar{\mathcal{A}}_{\mu\mu}^{FB}\right)_{\text{bin1}} &= \Big[-9.09 \pm 0.83_{\text{scale}} \pm 0.03_{m_t} \pm 0.24_{m_{c,C}} \pm 0.20_{m_b} \pm 0.18_{\alpha_s(M_Z)} \pm 0.02_{\lambda_2} \Big] \% \\
&= \Big[-9.09 \pm 0.91 \Big] \% \,, \qquad (59) \\
\left(\bar{\mathcal{A}}_{ee}^{FB}\right)_{\text{bin1}} &= \Big[-8.14 \pm 0.80_{\text{scale}} \pm 0.03_{m_t} \pm 0.23_{m_{c,C}} \pm 0.19_{m_b} \pm 0.18_{\alpha_s(M_Z)} \pm 0.02_{\lambda_2} \Big] \% \\
&= \Big[-8.14 \pm 0.87 \Big] \% \,, \qquad (60) \\
\left(\bar{\mathcal{A}}_{\mu\mu}^{FB}\right)_{\text{bin2}} &= \Big[+7.80 \pm 0.55_{\text{scale}} \pm 0.02_{m_t} \pm 0.31_{m_{c,C}} \pm 0.34_{m_b} \pm 0.16_{\alpha_s(M_Z)} \pm 0.20_{\lambda_2} \Big] \% \\
&= \Big[+7.80 \pm 0.76 \Big] \% \,, \qquad (61) \\
\left(\bar{\mathcal{A}}_{ee}^{FB}\right)_{\text{bin2}} &= \Big[+8.27 \pm 0.47_{\text{scale}} \pm 0.02_{m_t} \pm 0.30_{m_{c,C}} \pm 0.33_{m_b} \pm 0.15_{\alpha_s(M_Z)} \pm 0.19_{\lambda_2} \Big] \% \\
&= \Big[+8.27 \pm 0.69 \Big] \% \,. \qquad (62)
\end{aligned}$$

The total error is obtained by adding the individual ones in quadrature. For the entire low-$\hat{s}$ region, we get

$$\begin{aligned}
\left(\bar{\mathcal{A}}_{\mu\mu}^{FB}\right)_{\text{low}} &= \Big[-1.50 \pm 0.78_{\text{scale}} \pm 0.02_{m_t} \pm 0.29_{m_{c,C}} \pm 0.27_{m_b} \pm 0.18_{\alpha_s(M_Z)} \pm 0.10_{\lambda_2} \Big] \% \\
&= \Big[-1.50 \pm 0.90 \Big] \% \,, \qquad (63) \\
\left(\bar{\mathcal{A}}_{ee}^{FB}\right)_{\text{low}} &= \Big[-0.86 \pm 0.73_{\text{scale}} \pm 0.01_{m_t} \pm 0.28_{m_{c,C}} \pm 0.26_{m_b} \pm 0.18_{\alpha_s(M_Z)} \pm 0.10_{\lambda_2} \Big] \% \\
&= \Big[-0.86 \pm 0.85 \Big] \% \,. \qquad (64)
\end{aligned}$$

The relative errors in the respective bins are considerably smaller than for the entire low-$\hat{s}$ region since the respective values in each bin are similar in size and of opposite sign.

4.5 Analysis of the zero of the FBA

The basic formula for the extraction of the zero is Eq. (19). We expand the two ratios separately in α_s, κ, λ_1 and λ_2, and keep all the terms as specified in section 2.4. It is understood that also the conversion of the mass scheme for the botton, the charm and the top quark is performed in the way described there. The results for q_0^2, the zero of the FBA in the low-s region, are

$$\begin{aligned}
(q_0^2)_{\mu\mu} &= \Big[3.50 \pm 0.10_{\text{scale}} \pm 0.002_{m_t} \pm 0.04_{m_{c,C}} \\
&\qquad \pm 0.05_{m_b} \pm 0.03_{\alpha_s(M_Z)} \pm 0.001_{\lambda_1} \pm 0.01_{\lambda_2} \Big] \,\text{GeV}^2 = (3.50 \pm 0.12)\,\text{GeV}^2 \,, \qquad (65) \\
(q_0^2)_{ee} &= \Big[3.38 \pm 0.09_{\text{scale}} \pm 0.002_{m_t} \pm 0.04_{m_{c,C}} \\
&\qquad \pm 0.04_{m_b} \pm 0.03_{\alpha_s(M_Z)} \pm 0.002_{\lambda_1} \pm 0.01_{\lambda_2} \Big] \,\text{GeV}^2 = (3.38 \pm 0.11)\,\text{GeV}^2 \,. \qquad (66)
\end{aligned}$$

	1S	$\overline{\rm MS}$	pole
μ	3.50	3.47	3.52
e	3.38	3.34	3.41

Table 2: Dependence of the zero of the FBA on the b quark mass scheme. The input values are $\overline{m}_b(\overline{m}_b) = 4.205\,\text{GeV}$ [46] and $m_{b,\text{pole}} = 4.8\,\text{GeV}$.

The central values are obtained for the matching scale $\mu_0 = 120$ GeV and the low-energy scale $\mu_b = 5$ GeV. The uncertainty from missing higher order perturbative corrections have been estimated by increasing and decreasing the scales μ_0 and μ_b by factors of 2. Uncertainties induced by m_t, m_b, m_c, C, $\alpha_s(M_Z)$, λ_1 and λ_2 are obtained by varying the various inputs within the errors given in Table 1. We assume the errors on C and m_c to be fully correlated. The total errors are again obtained by adding the individual ones in quadrature. In order to show the stability of the zero under change of the b quark mass scheme we collect in Table 2 the results we obtained in the 1S, $\overline{\rm MS}$ and pole schemes.

The total errors are 3.4% and 3.3% respectively and therefore quite small. It is often argued that especially the small μ dependence at the zero is an accident and should be increased by hand. We argue in the following that the small μ dependence is a reasonable reflection of the perturbative error.

One test of our estimation of the perturbative error on the zero consists in comparing the central values and μ_b dependences of lower–order predictions. The comparison between the NNLO+QED, NNLO and NLO extraction of the zero reads (here we consider only the muon channel and quote only the scale uncertainty):

$$q_0^2 \;=\; \begin{cases} (3.50 \pm 0.10)\ \text{GeV}^2 & \text{NNLO + QED} \\ (3.45 \pm 0.11)\ \text{GeV}^2 & \text{NNLO} \\ (3.11 \pm 0.39)\ \text{GeV}^2 & \text{NLO} \quad . \end{cases} \tag{67}$$

In Fig. 2, we plot the μ_b dependence of the FBA in the low-q^2 region and compare NNLO and NLO QCD results. Here we note that the scale uncertainty is maximal at $q^2 \sim 1$ GeV^2, decreases smoothly at larger q^2 and almost vanishes at the edge of the low-q^2 region. Moreover, the band between the two solid lines, representing the scale uncertainty of the NNLO FBA, lies to a large extent within the shaded area of the NLO scale uncertainty. The same holds true if we compared NNLO+QED vs. NLO QCD results.

In Fig. 3 we show the entire – parametric and perturbative – error band of the full NNLO+QED asymmetry over the whole low-s region. The plot shows that the perturbative expansion converges nicely everywhere in the low-q^2 region.

The numerical results of Eq. (67) and the plots therefore suggest that the variation of the scale μ_b properly describes the size of the missing perturbative corrections.

As already stressed before, the errors considered here are parametric and perturbative ones

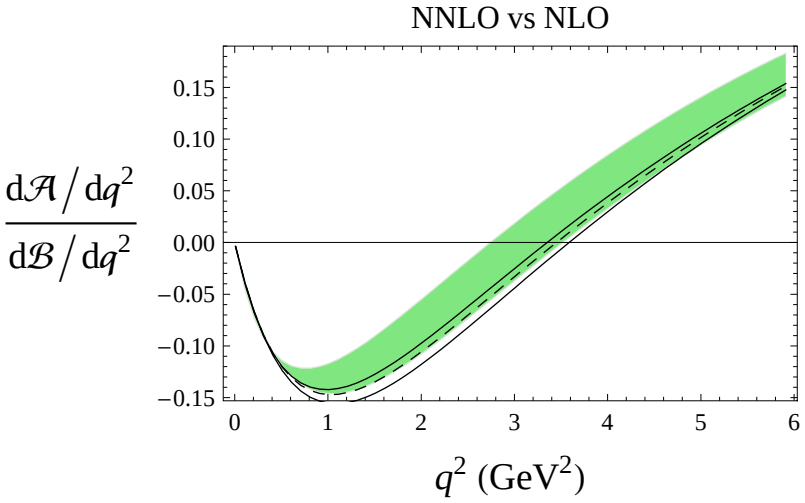

Figure 2: μ_b-dependence of the forward backward asymmetry for the muonic final state. The lines are the NNLO QCD result; the dashed line corresponds to $\mu_b = 5$ GeV, and the solid lines to $\mu_b = 2.5, 10$ GeV. The shaded area is the region spanned by the NLO asymmetry for 2.5 GeV $< \mu_b <$ 10 GeV.

only; and unknown subleading nonperturbative corrections of order $O(\alpha_s\Lambda/m_b)$ may give an additional uncertainty of order 5%.

4.6 New-physics formulae

Here, we present numerical formulae for the various observables for non-SM values of the high-scale Wilson coefficients of the operators P_7, P_8, P_9 and P_{10}:

$$\begin{aligned}
\mathcal{B}^{\rm high}_{\mu\mu} &= \Big[\, 2.399 - 0.002576\,\mathcal{I}(\delta R_{10}) - 0.01277\,\mathcal{I}(\delta R_7) + 0.0002656\,\mathcal{I}(\delta R_7\delta R_8^*) \\
&\quad +0.0004108\,\mathcal{I}(\delta R_7\delta R_9^*) + 0.002027\,\mathcal{I}(\delta R_8) - 0.00003375\,\mathcal{I}(\delta R_8\delta R_{10}^*) \\
&\quad +0.001676\,\mathcal{I}(\delta R_8\delta R_9^*) + 0.1079\,\mathcal{I}(\delta R_9) + 3.022\,\mathcal{R}(\delta R_{10}) + 0.001146\,\mathcal{R}(\delta R_{10}\delta R_7^*) \\
&\quad +0.0001236\,\mathcal{R}(\delta R_{10}\delta R_8^*) - 0.0173\,\mathcal{R}(\delta R_{10}\delta R_9^*) - 0.1312\,\mathcal{R}(\delta R_7) - 0.0143\,\mathcal{R}(\delta R_8) \\
&\quad +0.0008111\,\mathcal{R}(\delta R_8\delta R_7^*) + 0.9375\,\mathcal{R}(\delta R_9) - 0.0568\,\mathcal{R}(\delta R_9\delta R_7^*) \\
&\quad -0.006099\,\mathcal{R}(\delta R_9\delta R_8^*) + 1.558\,|\delta R_{10}|^2 + 0.003436\,|\delta R_7|^2 + 0.00004162\,|\delta R_8|^2 \\
&\quad +0.2231\,|\delta R_9|^2 \,\Big] \times 10^{-7}\,, \qquad (68) \\
\mathcal{B}^{\rm high}_{ee} &= \Big[\, 2.085 - 0.002576\,\mathcal{I}(\delta R_{10}) - 0.011\,\mathcal{I}(\delta R_7) + 0.0002656\,\mathcal{I}(\delta R_7\delta R_8^*) \\
&\quad +0.0004108\,\mathcal{I}(\delta R_7\delta R_9^*) + 0.002162\,\mathcal{I}(\delta R_8) - 0.00003375\,\mathcal{I}(\delta R_8\delta R_{10}^*) \\
&\quad +0.001676\,\mathcal{I}(\delta R_8\delta R_9^*) + 0.09845\,\mathcal{I}(\delta R_9) + 2.73\,\mathcal{R}(\delta R_{10}) + 0.001146\,\mathcal{R}(\delta R_{10}\delta R_7^*) \\
&\quad +0.0001236\,\mathcal{R}(\delta R_{10}\delta R_8^*) - 0.0173\,\mathcal{R}(\delta R_{10}\delta R_9^*) - 0.1119\,\mathcal{R}(\delta R_7) - 0.01279\,\mathcal{R}(\delta R_8) \\
&\quad +0.0006912\,\mathcal{R}(\delta R_8\delta R_7^*) + 0.8243\,\mathcal{R}(\delta R_9) - 0.04872\,\mathcal{R}(\delta R_9\delta R_7^*)
\end{aligned}$$

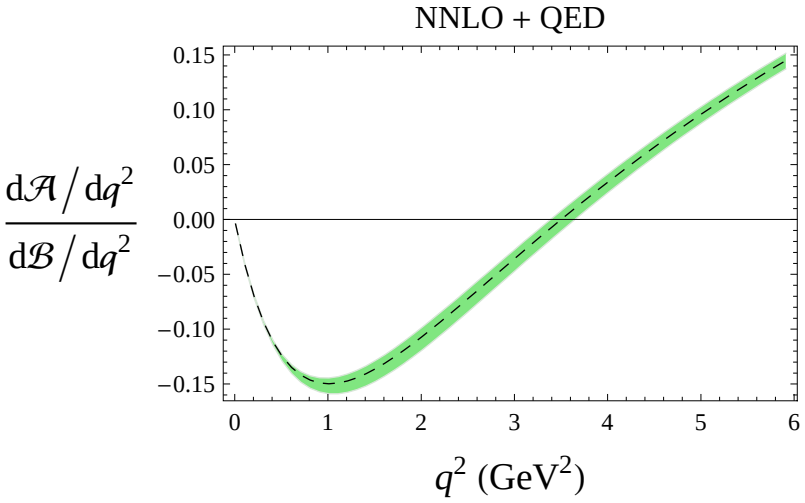

Figure 3: The full NNLO+QED asymmetry (dashed line) and the total – parametric and perturbative – error band (shaded area).

$$
\begin{aligned}
&-0.005478\,\mathcal{R}(\delta R_9 \delta R_8^*) + 1.411\,|\delta R_{10}|^2 + 0.002655\,|\delta R_7|^2 + 0.00003702\,|\delta R_8|^2 \\
&+0.2016\,|\delta R_9|^2\,\Big]\times 10^{-7}\,, \qquad (69)
\end{aligned}
$$

where

$$
1+\delta R_{7,8} = \frac{C_{7,8}^{(00)\mathrm{eff}}(\mu_0)}{C_{7,8}^{(00)\mathrm{eff,SM}}(\mu_0)} \qquad \text{and} \qquad 1+\delta R_{9,10} = \frac{C_{9,10}^{(11)}(\mu_0)}{C_{9,10}^{(11)\mathrm{SM}}(\mu_0)}\,, \qquad (70)
$$

and we refer the reader to the definition of the Wilson coefficients given in Ref. [28].

The analogous formulae for the integrated forward backward asymmetry in bin 1 and bin 2 are (we give separately the FBA from Eq. (10), $\mathcal{A}_{\mu\mu}^{FB}$, and the normalizing branching ratio from Eq. (3), $\mathcal{B}_{\mu\mu}$):

$$
\begin{aligned}
\left(\mathcal{A}_{\mu\mu}^{FB}\right)_{\mathrm{bin1}} \;=\; &\Big[\; -7.877 - 0.84\,\mathcal{I}(\delta R_{10}) + 0.1901\,\mathcal{I}(\delta R_8) + 0.1901\,\mathcal{I}(\delta R_8 \delta R_{10}^*) \\
&+0.02323\,\mathcal{I}(\delta R_9) - 8.136\,\mathcal{R}(\delta R_{10}) + 0.02323\,\mathcal{I}(\delta R_9)\,\mathcal{R}(\delta R_{10}) \\
&-6.114\,\mathcal{R}(\delta R_{10}\delta R_7^*) - 0.6183\,\mathcal{R}(\delta R_{10}\delta R_8^*) + 5.048\,\mathcal{R}(\delta R_{10}\delta R_9^*) \\
&-5.942\,\mathcal{R}(\delta R_7) - 0.6059\,\mathcal{R}(\delta R_8) + 4.947\,\mathcal{R}(\delta R_9) - 0.02323\,\mathcal{I}(\delta R_{10})\,\mathcal{R}(\delta R_9) \\
&+0.01569\,\mathcal{R}(\delta R_9 \delta R_7^*) - 0.08693\,|\delta R_{10}|^2 - 0.0128\,|\delta R_9|^2\,\Big]\times 10^{-8}\,, \qquad (71)
\end{aligned}
$$

$$
\begin{aligned}
\left(\mathcal{B}_{\mu\mu}\right)_{\mathrm{bin1}} \;=\; &\Big[\, 8.653 + 0.07321\,\mathcal{I}(\delta R_7) + 0.0167\,\mathcal{I}(\delta R_7 \delta R_8^*) + 0.002753\,\mathcal{I}(\delta R_7 \delta R_9^*) \\
&-0.003923\,\mathcal{I}(\delta R_8) + 0.01471\,\mathcal{I}(\delta R_8 \delta R_9^*) - 0.03578\,\mathcal{I}(\delta R_9) + 10.62\,\mathcal{R}(\delta R_{10}) \\
&+0.008387\,\mathcal{R}(\delta R_{10}\delta R_7^*) + 0.001049\,\mathcal{R}(\delta R_{10}\delta R_8^*) - 0.05413\,\mathcal{R}(\delta R_{10}\delta R_9^*)
\end{aligned}
$$

$$
\begin{aligned}
&+0.262\,\mathcal{R}(\delta R_7) + 0.02037\,\mathcal{R}(\delta R_8) + 0.05047\,\mathcal{R}(\delta R_8 \delta R_7^*) + 2.264\,\mathcal{R}(\delta R_9) \\
&-0.4778\,\mathcal{R}(\delta R_9 \delta R_7^*) - 0.05645\,\mathcal{R}(\delta R_9 \delta R_8^*) + 5.463\,|\delta R_{10}|^2 + 0.2087\,|\delta R_7|^2 \\
&+0.002892\,|\delta R_8|^2 + 0.7634\,|\delta R_9|^2\,\Big]\times 10^{-7}\,, \qquad (72)
\end{aligned}
$$

$$
\begin{aligned}
\left(\mathcal{A}_{\mu\mu}^{FB}\right)_{\rm bin2} &= \Big[\,5.459 - 0.7026\,\mathcal{I}(\delta R_{10}) + 0.1426\,\mathcal{I}(\delta R_8) + 0.1426\,\mathcal{I}(\delta R_8 \delta R_{10}^*) \\
&+0.03706\,\mathcal{I}(\delta R_9) + 5.472\,\mathcal{R}(\delta R_{10}) + 0.03706\,\mathcal{I}(\delta R_9)\,\mathcal{R}(\delta R_{10}) \\
&-4.48\,\mathcal{R}(\delta R_{10} \delta R_7^*) - 0.4645\,\mathcal{R}(\delta R_{10} \delta R_8^*) + 7.832\,\mathcal{R}(\delta R_{10} \delta R_9^*) \\
&-4.352\,\mathcal{R}(\delta R_7) - 0.4645\,\mathcal{R}(\delta R_8) + 7.622\,\mathcal{R}(\delta R_9) - 0.03706\,\mathcal{I}(\delta R_{10})\,\mathcal{R}(\delta R_9) \\
&+0.01172\,\mathcal{R}(\delta R_9 \delta R_7^*) - 0.1382\,|\delta R_{10}|^2 - 0.02034\,|\delta R_9|^2\,\Big]\times 10^{-8}\,, \qquad (73)
\end{aligned}
$$

$$
\begin{aligned}
\left(\mathcal{B}_{\mu\mu}\right)_{\rm bin2} &= \Big[\,7.052 + 0.02856\,\mathcal{I}(\delta R_7) + 0.005661\,\mathcal{I}(\delta R_7 \delta R_8^*) + 0.002082\,\mathcal{I}(\delta R_7 \delta R_9^*) \\
&+0.01401\,\mathcal{I}(\delta R_8) + 0.01112\,\mathcal{I}(\delta R_8 \delta R_9^*) - 0.03512\,\mathcal{I}(\delta R_9) + 9.472\,\mathcal{R}(\delta R_{10}) \\
&+0.006338\,\mathcal{R}(\delta R_{10} \delta R_7^*) - 0.04942\,\mathcal{R}(\delta R_{10} \delta R_9^*) - 0.4596\,\mathcal{R}(\delta R_7) \\
&-0.05505\,\mathcal{R}(\delta R_8) + 0.01678\,\mathcal{R}(\delta R_8 \delta R_7^*) + 2.394\,\mathcal{R}(\delta R_9) \\
&-0.3527\,\mathcal{R}(\delta R_9 \delta R_7^*) - 0.04016\,\mathcal{R}(\delta R_9 \delta R_8^*) + 4.879\,|\delta R_{10}|^2 \\
&+0.07016\,|\delta R_7|^2 + 0.6891\,|\delta R_9|^2\,\Big]\times 10^{-7}\,. \qquad (74)
\end{aligned}
$$

The integrated asymmetries in bin 1, bin 2, and in the whole low-q^2 region are then according to Eq. (19):

$$
\left(\bar{\mathcal{A}}_{\mu\mu}^{FB}\right)_{\rm bin1} = \frac{\left(\mathcal{A}_{\mu\mu}^{FB}\right)_{\rm bin1}}{\left(\mathcal{B}_{\mu\mu}\right)_{\rm bin1}}\,, \qquad (75)
$$

$$
\left(\bar{\mathcal{A}}_{\mu\mu}^{FB}\right)_{\rm bin2} = \frac{\left(\mathcal{A}_{\mu\mu}^{FB}\right)_{\rm bin2}}{\left(\mathcal{B}_{\mu\mu}\right)_{\rm bin2}}\,, \qquad (76)
$$

$$
\left(\bar{\mathcal{A}}_{\mu\mu}^{FB}\right)_{\rm low} = \frac{\left(\mathcal{A}_{\mu\mu}^{FB}\right)_{\rm bin1} + \left(\mathcal{A}_{\mu\mu}^{FB}\right)_{\rm bin2}}{\left(\mathcal{B}_{\mu\mu}\right)_{\rm bin1} + \left(\mathcal{B}_{\mu\mu}\right)_{\rm bin2}}\,. \qquad (77)
$$

5 Summary and Outlook

In this paper we extend the analysis of log–enhanced QED corrections initiated in Ref. [28] to the $\bar{B} \to X_s \ell\ell$ decay width in the high-q^2 region and to the forward backward asymmetry.

We give a complete phenomenological analysis of all relevant quantities related to these observables, including the ratio $\mathcal{R}(s_0)$ recently proposed in Refs. [24, 47]. We propose a new approach to the extraction of the zero of the FBA and argue that the scale dependence obtained by this procedure is a reasonable reflection of the perturbative error.

It is well-known that the measurements of those quantities, in addition to the $\bar{B} \to X_s\gamma$ branching ratio, will allow to fix magnitude and sign of all relevant Wilson coefficients in the

SM. Since at the end of the current B factories quantities integrated over certain q^2-bins will be already accessible with high precision, the following observation is important, namely that the double differential decay width decomposed according to ($z = \cos\theta$)

$$\frac{d^2\Gamma}{dq^2\,dz} = \frac{3}{8}\left[(1+z^2)\,H_T(q^2) \;+\; 2\,z\,H_A(q^2) + 2\,(1-z^2)\,H_L(q^2)\right]\,, \tag{78}$$

where

$$\frac{d\Gamma}{dq^2} = H_T(q^2) \;+ H_L(q^2)\,, \qquad \frac{dA_{\rm FB}}{dq^2} = 3/4\,H_A(q^2)\,, \tag{79}$$

includes a third quantity which depends on a different combination of Wilson coefficients [48]. The NNLO+QED analysis of this observable will be published in a forthcoming paper.

Acknowledgments

We would like to thank Martin Beneke, Christoph Greub, Ulrich Haisch, Gino Isidori, Mikołaj Misiak, Lalit Sehgal, and Peter Uwer for interesting and helpful discussions and suggestions. This work was supported by Schweizerischer Nationalfonds (SNF) and by Deutsche Forschungsgemeinschaft, SFB/TR 9 "Computergestützte Theoretische Teilchenphysik". Fermilab is operated by Fermi Research Alliance, LLC under Contract No. DE-AC02-07CH11359 with the United States Department of Energy.

References

[1] T. Hurth, Int. J. Mod. Phys. A **22** (2007) 1781 [arXiv:hep-ph/0703226].

[2] T. Hurth, Rev. Mod. Phys. **75** (2003) 1159 [arXiv:hep-ph/0212304].

[3] M. Iwasaki *et al.* [Belle Collaboration], hep-ex/0503044.

[4] B. Aubert *et al.* [BABAR Collaboration], Phys. Rev. Lett. **93** (2004) 081802 [hep-ex/0404006].

[5] C. Bobeth, M. Misiak and J. Urban, Nucl. Phys. B **574** (2000) 291 [hep-ph/9910220].

[6] H. H. Asatryan, H. M. Asatrian, C. Greub and M. Walker, Phys. Rev. D **65** (2002) 074004 [hep-ph/0109140].

[7] H. H. Asatryan, H. M. Asatrian, C. Greub and M. Walker, Phys. Rev. D **66** (2002) 034009 [hep-ph/0204341].

[8] A. Ghinculov, T. Hurth, G. Isidori and Y. P. Yao, Nucl. Phys. B **648** (2003) 254 [hep-ph/0208088].

[9] H. M. Asatrian, K. Bieri, C. Greub and A. Hovhannisyan, Phys. Rev. D **66** (2002) 094013 [hep-ph/0209006].

[10] A. Ghinculov, T. Hurth, G. Isidori and Y. P. Yao, Eur. Phys. J. C **33** (2004) S288 [arXiv:hep-ph/0310187].

[11] A. Ghinculov, T. Hurth, G. Isidori and Y. P. Yao, Nucl. Phys. B **685** (2004) 351 [hep-ph/0312128].

[12] C. Bobeth, P. Gambino, M. Gorbahn and U. Haisch, JHEP **0404**, 071 (2004) [hep-ph/0312090].

[13] H. M. Asatrian, H. H. Asatryan, A. Hovhannisyan and V. Poghosyan, Mod. Phys. Lett. A **19** (2004) 603 [arXiv:hep-ph/0311187].

[14] M. Gorbahn and U. Haisch, Nucl. Phys. B **713** (2005) 291 [hep-ph/0411071].

[15] A. G. Akeroyd et al., arXiv:hep-ex/0406071.

[16] J. Hewett et al., arXiv:hep-ph/0503261.

[17] M. Bona *et al.*, arXiv:0709.0451 [hep-ex].

[18] A. F. Falk, M. E. Luke and M. J. Savage, Phys. Rev. D **49**, 3367 (1994) [arXiv:hep-ph/9308288].

[19] A. Ali, G. Hiller, L. T. Handoko and T. Morozumi, Phys. Rev. D **55**, 4105 (1997) [hep-ph/9609449].

[20] J. W. Chen, G. Rupak and M. J. Savage, Phys. Lett. B **410**, 285 (1997) [hep-ph/9705219].

[21] G. Buchalla, G. Isidori and S. J. Rey, Nucl. Phys. B **511**, 594 (1998) [arXiv:hep-ph/9705253].

[22] G. Buchalla and G. Isidori, Nucl. Phys. B **525**, 333 (1998) [hep-ph/9801456].

[23] C. W. Bauer and C. N. Burrell, Phys. Rev. D **62**, 114028 (2000) [hep-ph/9911404].

[24] Z. Ligeti and F. J. Tackmann, Phys. Lett. B **653** (2007) 404 [arXiv:0707.1694v2].

[25] F. Kruger and L. M. Sehgal, Phys. Lett. B **380** (1996) 199 [arXiv:hep-ph/9603237].

[26] K. S. M. Lee and I. W. Stewart, Phys. Rev. D **74** (2006) 014005 [hep-ph/0511334].

[27] K. S. M. Lee, Z. Ligeti, I. W. Stewart and F. J. Tackmann, Phys. Rev. D **74** (2006) 011501 [hep-ph/0512191].

[28] T. Huber, E. Lunghi, M. Misiak and D. Wyler, Nucl. Phys. B **740** (2006) 105 [hep-ph/0512066].

[29] C. W. Bauer, Z. Ligeti, M. Luke, A. V. Manohar and M. Trott, Phys. Rev. D **70**, 094017 (2004) [hep-ph/0408002].

[30] I. Blokland, A. Czarnecki, M. Slusarczyk and F. Tkachov, Phys. Rev. D **71** (2005) 054004 [arXiv:hep-ph/0503039].

[31] M. B. Voloshin, Phys. Lett. B **515**, 74 (2001) [arXiv:hep-ph/0106040].

[32] A. Ali, T. Mannel and T. Morozumi, Phys. Lett. B **273** (1991) 505.

[33] A. H. Hoang, Z. Ligeti and A. V. Manohar, Phys. Rev. D **59** (1999) 074017 [hep-ph/9811239].

[34] A. H. Hoang, hep-ph/0008102.

[35] A. Czarnecki and K. Melnikov, Phys. Rev. Lett. **88**, 131801 (2002) [arXiv:hep-ph/0112264].

[36] K. G. Chetyrkin, R. Harlander, T. Seidensticker and M. Steinhauser, Phys. Rev. D **60** (1999) 114015 [arXiv:hep-ph/9906273].

[37] I. Blokland, A. Czarnecki, M. Slusarczyk and F. Tkachov, Phys. Rev. Lett. **93**, 062001 (2004) [arXiv:hep-ph/0403221].

[38] S. Bethke, Prog. Part. Nucl. Phys. **58**, 351 (2007) [arXiv:hep-ex/0606035].

[39] J. Charles *et al.* [CKMfitter Group], Eur. Phys. J. C **41**, 1 (2005) [hep-ph/0406184].

[40] A. H. Hoang and A. V. Manohar, hep-ph/0509195.

[41] B. Aubert *et al.* (BaBar Collaboration), Phys. Rev. Lett. **93**, 011803 (2004) [hep-ex/0404017].

[42] P. A. Movilla Fernandez [CDF Collaboration], arXiv:0705.3910 [hep-ex].

[43] S. Eidelman *et al.* [Particle Data Group], Phys. Lett. B **592**, 1 (2004).

[44] J. Berryhill, A. Ishikawa, private communication.

[45] A. Ali, E. Lunghi, C. Greub and G. Hiller, Phys. Rev. D **66** (2002) 034002 [arXiv:hep-ph/0112300].

[46] R. Boughezal, M. Czakon and T. Schutzmeier, Phys. Rev. D **74** (2006) 074006 [arXiv:hep-ph/0605023].

[47] C. W. Bauer, Z. Ligeti and M. E. Luke, Phys. Lett. B **479** (2000) 395 [arXiv:hep-ph/0002161].

[48] K. S. M. Lee, Z. Ligeti, I. W. Stewart and F. J. Tackmann, Phys. Rev. D **75** (2007) 034016 [arXiv:hep-ph/0612156].